2026-03-11
The self-archived postprint version of this journal article is available at Linköping University Institutional Repository (DiVA):
https://urn.kb.se/resolve?urn=urn:nbn:se:liu:diva-198858

Mononuclear copper(i) complexes bearing a 3-phenyl-5-(pyridin-4-yl)-1,2,4-triazole ligand: synthesis, crystal structure, TADF-luminescence, and mechanochromic effects

Alexey Gusev, Elena Braga, Ekaterina Zamnius, Mikhail Kiskin, Amjad Ali, Glib Baryshnikov and Wolfgang Linert

Dalton Transactions, (2023), 52(41), pp. 14995-15008.
Publisher: Royal Society of Chemistry
https://doi.org/10.1039/d3dt02633g

N.B.: When citing this work, cite the original publication.

Copyright holder: See original publication

LINKÖPING UNIVERSITY

ARTICLE

Mononuclear copper(I) complexes bearing 3-phenyl-5-(pyridin-4-yl)-1,2,4-triazole ligand: synthesis, crystal structure, TADF-luminescence, and mechanochromic effects

Received 00th January 20xx,
Accepted 00th January 20xx

DOI: 10.1039/x0xx00000x

Alexey Gusev *[a], Elena Braga [a], Ekaterina Zamnius [a], Mikhail Kiskin [b], Amjad Ali [c], Glib Baryshnikov *[c], Wolfgang Linert *[d]

Three new mononuclear heteroleptic copper(I) halide complexes, $[CuL(PPh_3)_2X]$ (X = Cl, Br, I), based on 3-phenyl-5-(pyridin-4-yl)-1,2,4-triazole (L) and triphenylphosphine (PPh_3) ligands, have been prepared by reaction of CuX (X = Cl, Br, I), L and PPh_3 in a molar ratio of 1:1:2 in MeCN solutions. Synthesized complexes exhibit blue light emission in solutions and bright green emission in the crystal state with quantum yields up to 100%. The luminescence decay analysis and density functional theory calculations revealed that the emission of solid samples at room temperature corresponds to the thermally activated delayed fluorescence while those at 77 K is assigned to phosphorescence. Utilizing the studied complexes in OLED heterostructures resulted in high-performing green-emitting devises with external quantum efficiency up to 13.4%.

Introduction

In the last decade color tunable luminescent materials have attracted increasing attention for light emitting devices, sensing devices, solar cells, and artificial photosynthesis[1-7]. Though there are numerous *d* transition metal ions in various oxidation states, the ions commonly utilized in these studies are mostly limited to the d^6, d^8, and d^{10} ions, representative ones of which are Ir(III)[8-11], Pt(II)[12-14], and Zn(II)[15-18] and Cu(I) ions[19-23], respectively. Despite considerable advances in recent decades in the synthesis, radiation efficiency and practical use of luminescent *d*-metal complexes, the development of industrially relevant devices based on them remains an unsolved problem, primarily due to the high cost and low abundance of traditional heavy-atom-based phosphorescent materials, such as platinum, osmium, or iridium. From these reasons luminescent Cu(I) complexes represent a cheaper alternative to the traditional platinum group metal complexes[24]. Rich coordination chemistry of Cu(I) ions makes it possible to perform fine-tuning of emission properties by variation of organic and inorganic ligands. Moreover the emission of Cu(I) complexes can be tuned not only using their structure and composition, but it can also be affected by external stimuli. Indeed, such compounds could exhibit a solvato-, thermo- and mechanochromism behaviors, displaying different luminescence responses when interact with solvent molecules or due to physical stimuli such as changes in temperature/pressure, phase dispersion degree, etc.[24-27]

For copper(I) complexes, due to the d^{10} electronic configuration, non-emissive and photodissociative processes related to the occupancy of d-d* states cannot be realized. However, the photochemistry of copper(I) halide complexes with mixed organic ligands is quite complicated. Apart from the intraligand transitions typical for closed-shell metal complexes, the MLCT (metal-to-ligand charge transfer), XLCT (halide-to-ligand charge transfer) transitions are often observed. In addition the so-called cluster-centered transitions are also possible for polynuclear complexes[23,28] .

Considerable interest to copper(I) complexes has been recently shown to be driven by the possibility of thermal activated delayed fluorescence (TADF) based on the equilibrium between the (^{1}MLCT) singlet and (^{3}MLCT) triplet states realized at small (about 1000 cm^{-1}) energy gaps between these states. As a result, such TADF emission complexes allow to get 100% internal quantum efficiency when utilized in OLEDs.[29]

Most of the mononuclear Cu(I) complexes have a pseudotetrahedral geometry, which always undergoes the Jahn-Teller distortion in excited state through metal-to-ligand charge transfer process.[30, 31] Such rearrangement usually results in low phosphorescence quantum yield. Given that the energy of MLCT states is largely determined by the electronic structure of organic ligands, the photophysical properties of copper complexes can be relatively simply tuned by successfully selecting the closest environment of the central atom.

[a] *Crimean Federal University, Simferopol, 295007, Crimea.*
[b] *N.S. Kurnakov Institute of General and Inorganic Chemistry, Russian Academy of Sciences, Moscow, Russia.*
[c] *Linköping University, Department of Science and Technology, Laboratory of Organic Electronics, Norrköping, SE-60174, Sweden*
[d] *. Institute of Applied Synthetic Chemistry, Vienna University of Technology, Getreidemarkt 9/163-AC, A-1060 Vienna, Austria*

Electronic Supplementary Information (ESI) available: [Crystallographic, OLED preparation and computational details, tables of crystal and refinement data for; IR-spectra, CIE coordianates .CCDC 2271720-2271722 contains supplementary crystallographic data for compounds 1-3, respectively]. See DOI: 10.1039/x0xx00000x

Please do not adjust margins

Moreover, in addition to electronic factors, steric and supramolecular factors, which prevent the distortion of the coordination polyhedron geometry, thereby reducing nonradiation energy losses and increasing the quantum yield of luminescence, also have a great impact. Thus, the molecular design of ligands to organize the optimal arrangement of ligands around the copper central atom is a non-trivial challenge for coordination chemistry.

A general strategy for constructing Cu(I)-based TADF materials exploits diverse ligands of N-, P- or mixed N,P-type, often with halide co-ligands. Among N-donor ligands pyridine derivatives as well as derivatives of 1,10-phenanthroline and 2,2'-dipyridyl are the most popular.[32] Nevertheless, the search for new heterocyclic systems is actively conducted in order to optimize the photophysical properties of copper complexes. One of those systems contain pyridine rings connected to a 5-membered N-heterocycle include a number of triazole and tetrazole derivatives[29]. Recently, Xu et al. have reported the TADF Cu(I) emitters based on N-ligands of 3-phenyl-5-(pyridin-2-yl)-1,2,4-triazole[33] family.

Herein, we have demonstrate that 4-pyridyl derivatives of 1,2,4-triazole can be also used to design Cu(I) TADF emitters. We report the synthesis and characterization of three mononuclear Cu(I) halide complexes $[CuX(PPh_3)_2(L)]$ (X = Cl^-, Br^-, I^-; L = 3-phenyl-5-(pyridin-4-yl)-1,2,4-triazole, PPh_3 = triphenylphosphine). Obtained complexes demonstrate high efficiency of emission at room temperature due to TADF mechanism of luminescence that was utilized in fabrication of high-performance OLEDs.

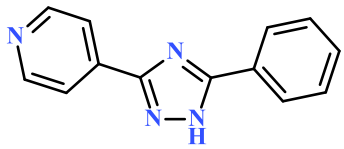

Figure 1. Chemical structure of 3-phenyl-5-(pyridin-4-yl)-1,2,4-triazole (L)

Experimental

Materials and physical methods. All reagents and solvents were commercially available (Sigma-Aldrich and Merck) and used as received without further purification. The 3-phenyl-5-(pyridin-4-yl)-1,2,4-triazole ligand was synthesized as described in our previous studies [34]. Elemental analyses of C, H, and N were performed with a EuroEA 3000 analyzer.

The IR spectra were measured by FSM 2202 spectrometer in the range of 4000-400 cm^{-1}. Absorption spectra were recorded with a Cintra-3000 spectrometer. ^1H NMR and ^{31}P NMR spectra were recorded on a Bruker Avance III 400 MHz NMR spectrometer.

Photoluminescence spectra of solid state samples were recorded on the FluoroMax-4 spectrometer. Absolute quantum yields at 298 were carried out with HORIBA Jobin-Yvon FluoroMax-4-equipped with an integrating sphere. The value of quantum yields shows the ca. 5 % fluctuation depending on the measurement conditions such as amount and size of samples. The QY values presented in this paper are the average of the three measurements. Quantum yields of luminescence (QY) at 77 K were measured relative to the quantum yield of the same sample at 300 K. Relative quantum yields were calibrated using the absolute QY values measured at 77 K.

Fluorescence decay lifetimes were measured using a Picoquant300 TCSPC. Phosphorescence decay lifetimes were measured using a "FLUORATE®-02-PANORAMA". Thermogravimetric and DSC analysis experiments were performed with a STA 6000 thermal analyser in the range 25-600°C (heating rate: 10 $K{\cdot}min^{-1}$) in air atmosphere. Cyclic voltammetry measurement for complexes 1-3 were performed following the protocol described in literature [35].

Synthesis

CuX (X – Cl, Br and I) (0.25 mmol) were added to solution of PPh_3 (133 mg, 0.5 mmol) and L (56 mg, 0.25 mmol) in dry CH_3CN (30 mL). Reaction mixture was stirred for 2 h at 60 °C under nitrogen atmosphere. The crude pale yellow solution was filtered to remove the insoluble impurity. Obtained clear solution was left to stay at room temperature. On the next day light-yellow prismatic crystals precipitated.

Light-yellow crystals $CuCl(PPh_3)_2L{\cdot}0.25CH_3CN$ (Complex 1) (yield 38 %). Elemental analysis found: C: 69.44; H: 4.58; N: 6.95%, calculated for $C_{49.5}H_{40.75}CuClN_{4.25}P_2$ C: 69.47; H: 4.77; N: 6.92 %. ^1H-NMR (400 MHz, $CDCl_3$): 11.1 (s, 1H), 8.57 (d, J = 6.4 Hz, 2H), 8.19 (d, J = 6.2 Hz, 2H), 7.88 (d, J = 7.0 Hz, 2H) 7.61-7.24 (m, 33H). ^{31}P-NMR (400 MHz, $CDCl_3$): δ −7.0.
IR (cm^{-1}): 3050 w, 2990 w, 1615 m, 1586 w, 1479 m, 1462 m, 1433 s, 1418 m, 1381 m, 1095 s, 981 m, 842 m, 743 s, 693 s, 509 s, 492 s, 353 (m), 283 m.

Light-yellow crystals $CuBr(PPh_3)_2L{\cdot}0.25CH_3CN$ (Complex 2) (yield 51 %). Elemental analysis found: C: 66.03; H: 4.70; N: 6.31%, calculated for $C_{49.5}H_{40.75}CuBrN_{4.25}P_2$ C: 65.96; H: 4.53; N: 6.60 %. ^1H-NMR (400 MHz, $CDCl_3$): 11.2 (s, 1H), 8.62 (d, J = 6.8 Hz, 2H), 8.22 (d, J = 5.6 Hz, 2H), 7.81 (d, J = 7.8 Hz, 2H) 7.68-7.21 (m, 33H). ^{31}P-NMR (400 MHz, $CDCl_3$): δ −6.7. IR (cm^{-1}): 3052 w, 3000 w, 1615 m, 1586 w, 1480 m, 1460 m, 1433 s, 1418 m, 1378 m, 1094 s, 981 m, 842 m, 742 s, 692 s, 516 s, 491 s, 284 m, 257(m).

Light-yellow crystals $CuI(PPh_3)_2L{\cdot}0.25CH_3CN$ (Complex 3) (yield 50 %). Elemental analysis found: C: 62.72; H: 4.51; N: 6.03%, calculated for $C_{49.5}H_{40.75}CuIN_{4.25}P_2$ C: 62.69; H: 4.30; N: 6.27%. ^1H-NMR (400 MHz, $CDCl_3$): 11.1 (s, 1H), 8.58 (d, J = 6.4 Hz, 2H), 8.31 (d, J = 5.8 Hz, 2H), 7.76 (d, J = 7.4 Hz, 2H), 7.68 (dd, J = 8.2 Hz, 2H), 7.54-7.24 (m, 31H). ^{31}P-NMR (400 MHz, $CDCl_3$): δ −6.5. IR (cm^{-1}): 3050 w, 2992 w, 1615 m, 1586 w, 1478 m, 1461 m, 1433 s, 1418 m, 1380 m, 1094 s, 981 m, 842 m, 743 s, 692 s, 518 s, 492 s, 289 m, 144(m)

X-ray Crystallography

Powder X-ray diffraction patterns were obtained with a Rigaku MiniFlex-II X-ray diffractometer with CuK/α radiation (λ=1.54178 Å). Single crystal X–ray diffraction data were collected using Bruker APEX II diffractometer (CCD detector, MoK/α radiation, λ = 0.71073 Å). Semi-empirical empirical absorption corrections for all complexes were applied [36]. The structure of the complexes were solved by the direct method and refined in the full-matrix anisotropic approximation for all non–hydrogen atoms. The hydrogen atoms of the carbon-

 This journal is © The Royal Society of Chemistry 20xx

Please do not adjust margins

Please do not adjust margins

containing ligands were positioned geometrically and refined using the riding model. The crystal structure was solved by using Olex2 packages and/or SHELXL-2014 [37] The crystallographic parameters and the structure refinement statistics for **1**-**3** are shown in **Table S1**.

Results and discussion

Synthesis and characterization of the complexes.

Copper-(I) halide complexes 1-3 were first prepared by treatment of cuprous halide with 2 equiv of PPh_3 in acetonitrile solution, followed by the addition of 1 equiv of 3-phenyl-5-(pyridin-4-yl)-1,2,4-triazole. The yields of 1-3 were 41-52%. Copper(I) halide complexes 1-3 are soluble in CH_3OH, and CH_3CN and only sparingly soluble in CH_2Cl_2. Moreover, 1-3 are air-stable in the solid state and for extended periods of time (up to 7 days) in solution. Obtained complexes were fully characterized by elemental analysis, NMR- spectroscopy, IR-spectroscopy, electronic absorption spectroscopy, luminescence spectroscopy, and single-crystal X-ray diffraction. The infrared spectra of 1-3 (Fig. S1) show all the characteristic bands typical for L and PPh_3. Aromatic bands of phenyl ring appear at 1615 cm^{-1}, while characteristic vibration bands of the triazole core were found in the range 1418–1480 cm^{-1}. Upon P-Cu(I) coordination, the characteristic ν(P-C_{Ph}) peak of PPh_3 in 1-3 occurs at slightly higher frequency (~1094 cm^{-1}) relative to that of free PPh_3 (1089 cm^{-1}) [39]. In the low-frequency region of the IR spectra of complexes 1-3, the Cu-N and Cu-X vibrations (X = Cl, Br, I) are highlighted, which indicates the coordination of triazole ligand and halide ions to copper atoms. The band corresponding to Cu-N vibrations in the spectra of all complexes is in the range of 283-289 cm^{-1}, and for Cu-X valence vibrations (in the range 144-353 cm^{-1}). For all studied complexes halide ions are terminal, so the ratio of the ν(Cu-Br)/ν(Cu-Cl) and ν(Cu-Cl)/ν(Cu-I) band vibrations agree well with the literature data.[38] According to thermogravimetric analysis, halide complexes 1-3 contain trace amount of acetonitrile molecules (0.1-0.25 mol CH_3CN per 1 mol of complex). They are thermally stable up to 220-230 °C (mass losses are 1.5-2% at 75-175 °C, which corresponds to the elimination of acetonitrile solvate molecules from the crystal lattice) (Fig. S2). At temperatures 215 (for 1), 211 (for 2), and 195 °C (for 3), the melting of samples is observed, which is accompanied by an extremum on the DSC curve. Further heating of the complexes leads to rapid loss of mass due to thermal decomposition of the complexes. Practically complete decomposition is achieved near 400 °C.

According to single crystal X-ray analysis, all synthesized complexes crystallize in triclinic space group $P\bar{1}$ as a solvate with 0.5 (for 1 and 3) and 0.25 (for 2) molecule of acetonitrile. Complexes 2 and 3 are isostructural while crystalline packing of complex 1 is slightly different. Figures 2 a, b, c show the molecular structures of 1, 2 and 3, respectively. In contrast to the previously described binuclear $[Cu_2I_2L_2(PPh_3)_2]$ complex[39] obtained similarly to complex 3, but with a reagent molar ratio of 1:1:1, the new complexes 1-3 have a mononuclear structure. The most relevant structural parameters of complexes 1-3 are presented in the Table S2. For all complexes, the central Cu atom coordinates one halide-anion, two P and one N, resulting in a NP_2X distorted tetrahedral geometry (τ_4 [40]= 0.87 for 1 and 0.89 for 2 and 3). The Cu–X (X – halide) bond lengths range from 2.4062(5) Å to 2.6602(7) Å, which are comparable to the values reported for mononuclear Cu(I) complexes [41, 42].

By comparing all three complexes, it is found that the X-Cu-P (X – Cl, Br or I) angles are obviously different, which may arise from steric hindrance between L and PPh_3. Triazole acts as a neutral monodentate ligand binding Cu ion through N-pyridine atom. The averaged planes of phenyl and pyridyl rings of the triazole ligand in Br and I derivatives are only slightly twisted relative to the plane of the triazole ring (angle between these rings is 7.08(16)° and 6.1(3)º for complexes 2 and 3, respectively). In the case of complex 1 coordinated L is considerably twisted. Torsion angle between pyridine and triazole rings as well as phenyl and triazole rings are equal to 23.54(13) and 11.68(14)° respectively. The distortion degree of the geometries suggests that photoluminescence properties of 1 would be differ from properties of 2 and 3.

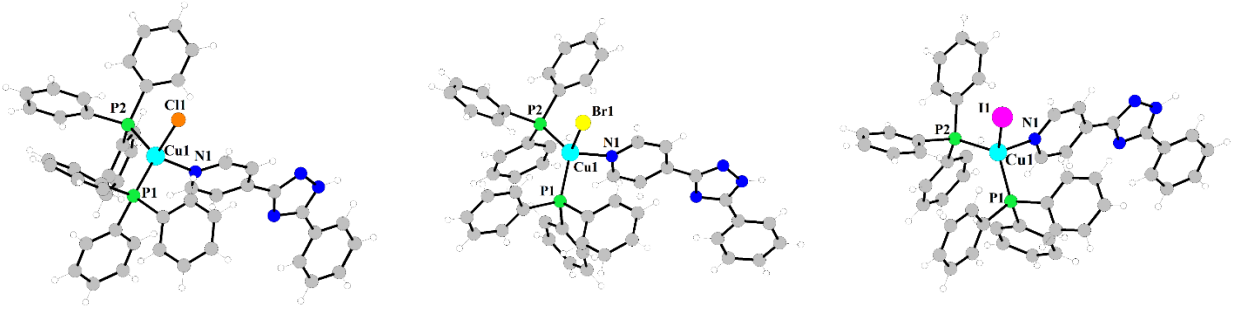

a b c

Please do not adjust margins

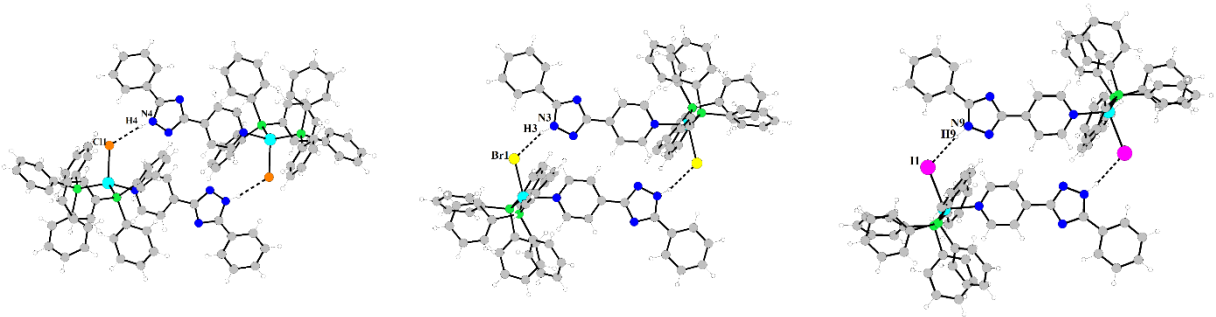

d e f

Figure 2. Molecular structures of complexes 1 (a), 2 (b) and 3 (c). Intermolecular interactions between neighboring complexes 1 (d), 2 (e) and 3 (f) in single crystal state.

The coordinated halide ion of neighbor molecules 1-3 acts as a hydrogen bond acceptor and forms a hydrogen bond with the triazole's NH-groups of the adjacent complex molecules (Fig. 2 d, e, f, Table S3). Such interaction leads to formation of supramolecular centrosymmetric dimers given intramolecular Cu…Cu distances of 11.128 (for 1), 11.285 (for 2) and 11.400 Å (for 3). In crystal 2 and 3, the phenyl and pyridyl fragments of L, as well as, phenyl rings of PPh_3 of neighboring molecules overlap each other, participating in π...π interaction (Table S4) and a the supramolecular layer structures.

Photophysical study.

The UV-Vis absorption spectra were measured in acetonitrile solution ($5 \cdot 10^{-5}$ M) (Fig. 3a). The absorption spectra of complexes 1-3 are very similar, showing an intense absorption band around 272-275 nm which is attributed to spin-allowed π-π* transitions within the phosphine ligands [41]. In addition second peak close to 301-303 nm is observed and assigned to π-π* transitions within the triazole ligand [39]. At low energy region, close to 370-385 nm a broad absorption band, which is mainly attributed to a metal-to-ligand charge-transfer (MLCT) transition.[34,43,44]

Luminescence spectra for the complexes 1-3 recorded in the solid state at room temperature and 77 K and in CH_3CN solution at 298 K, are shown in Figures 3 b, c; data are summarized in Table 1.

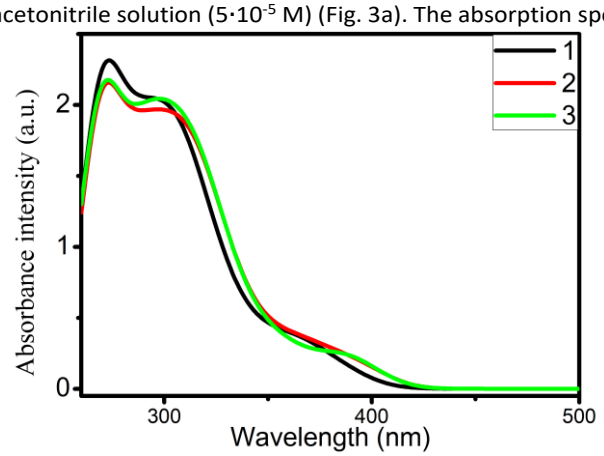

a

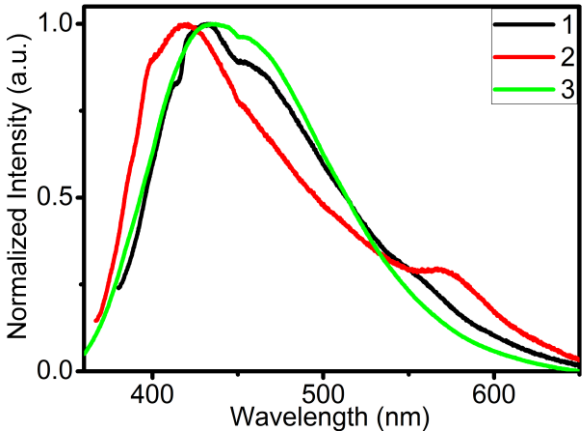

b

This journal is © The Royal Society of Chemistry 20xx

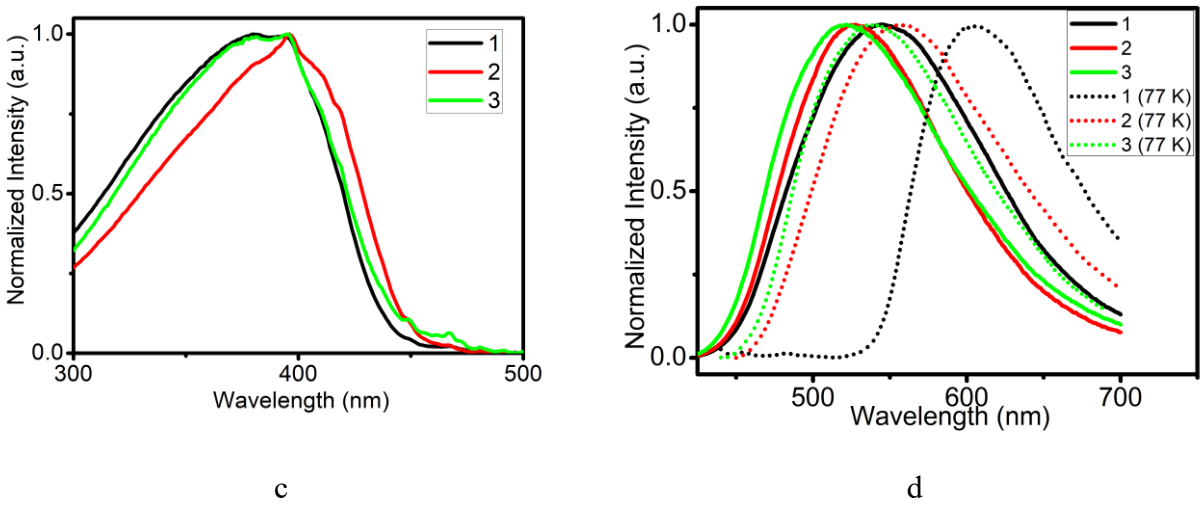

Figure 3. Absorption (a) and normalized emission (b) spectra of complexes 1-3 in CH_3CN (5·10-5 M) and normalized solid-state excitation (c) and emission (d) spectra of complexes 1-3.

In degassed acetonitrile solution at ambient temperature, complexes demonstrate broad emission band with main maxima peaking at 424, 431 and 456 nm for 1; 400, 419 and 452 nm for 2; 436 and 455 nm for 3. The luminescence quantum yield of 1-3 is 1.2, 0.8, and 0.9 %, respectively. The luminescence decay profiles of 1-3 were measured by monitoring main maxima of each complexes and fitting by double-exponential decay curves. Notably, luminescence average lifetimes of 1-3 were found to be in the range 12.9-15.4 ns that indicate fluorescent nature of emission corresponding to the intraligand transitions. A distinct feature of the spectra of the solutions of complexes 1 and 2 is the presence of a low-intensity band with a maximum at 543 (shoulder) and 567 nm, respectively. Analysis of the decay curve for complex 2 by the monitoring of band at 567 nm made it possible to determine the lifetime that equal to 1211 ns. This value indicates that the these bands might correspond to the phosphorescence of (M + X)LCT origin. It is quite possible that the emission properties of the complexes in solution represent a superposition of luminescence of both the complexes themselves and the products of their dissociation, dimerization, and oxidation, as in the case of many other Cu(I)-halide complexes [41, 42].

Table 1. Photophysical properties of complexes 1-3 in solution and in solid state at different temperatures.

Complex	**1**	**2**	**3**
CH_3CN solution			
λ_{max} (nm)	424, 431 and	400, 419, 452,	436 and 455
τ_{av} (ns)	456	567	15.4
QY (%)	12.9	13.2	0.9
	1.2	0.8	
Solid (crystalline form) 298 K			
λ_{max} (nm)	544	528	522
τ (μs)	13.2	3.72	3.0
QY (%)	58.8	70.3	29.1
k_r (s^{-1})	$4.37·10^4$	$1.88·10^5$	$9.08·10^4$
CIE	0.32:0.51	0.35:0.52	0.32:0.49
Solid (crystalline form) 77 K			
λ_{max} (nm)	603	555	541
τ (μs)	24.1	173.9	210.7
QY (%)	98.1	≈100	77.4
k_r (s^{-1})	$4.08·10^4$	$5.75·10^3$	$3.63·10^3$
ΔE(S-T) (cm^{-1})	1944	890	675

The excitation profiles of 1-3 (Fig. 3c) have a featureless shape that is also typical of Cu(I) complexes with MLCT-type emission.[29] Upon UV-excitation at 298 K, crystalline complexes 1-3 exhibit intense green photoluminescence, and the emission maxima were observed at 544, 528, and 522 nm for 1, 2, and 3, respectively. Commission Internationale d'Eclairage (CIE) coordinates are summarized in Table 3 and Figure S3. As shown in Figure 3 d, the emission spectra of these Cu(I) complexes in solid state are close similar with only slight blue shift in the row of Cl, Br, I derivatives. Decreasing the temperature to 77 K results in a bathochromic shift of the emission maxima to 603, 555, and 541 nm for Cl, Br, I derivatives, respectively. The red shift from 298 to 77 K is an indication of thermal activation of the energetically higher-lying S_1 state. All spectra of 1-3 at both 298 and 77 K are broad and unstructured, indicating that the emissive excited states have a MLCT character in this temperature range. [45]

The photoluminescence quantum yields for solid 1-3 in is 58 % for 1, 70 % for 2, and 29 % for 3 at 298 K, and by cooling to 77 K it became extremely high: 98% for 1, 100% for 2 and decreases to 77 % for 3. To further clarify the emission properties, the temperature dependence of the emission lifetimes of complexes was investigated. At room temperature the luminescence lifetimes of the complexes have proved to be single exponential in the range between between 3.2 μs (3) and 13.2 μs (1), and are comparable with the most Cu(I) emitters [46]. When the temperature was decreased to 77 K, the 2 and 3 solid samples showed a longer and monoexponential decay lifetime reaching 174 and 212 μs indicating phosphorescent origin of luminescence. In the case of complex 1, the lifetime increases insignificantly and at 77 K reaches 24 μs. Studying the decay time of complexes 2 and 3 as a function of temperature in the range between 77 K and 298 K, showing a sigmoidal profile of the τ vs. T curve that typical for the complexes with interplay between the TADF and phosphorescence processes upon temperature change. Furthermore, the radiative decay rate k_r

Please do not adjust margins

at room temperature are more than one order larger than those at 77 K. The k_r changes altogether with the blue shift by increasing temperature are attributed to a higher-lying energy emitting state. In this case, the ^{1}MLCT that carries a high radiative rate being thermally populated by a lower energy state, ^{3}MLCT, hence demonstrating the TADF behaviour. For thermally equilibrated states, the emission decay time of the two excited state system can be expressed as a function of the temperature expressed by a Boltzmann-type equation (1): [47, 48]

$$\tau(T) = \frac{3+\exp\left(-\frac{\Delta E}{k_B T}\right)}{\frac{3}{\tau(T_1)}+\frac{1}{\tau(S_1)}\exp\left(-\frac{\Delta E}{k_B T}\right)} \quad (1)$$

where ΔE is the energy gap between the singlet and triplet states, $\tau(S_1)$ and $\tau(T_1)$ are the lifetimes of S_1 (fluorescence) and T_1 (phosphorescence) states. Fitting of Eq. 1 to the experimental data of emission decay time of complexes lead to a good fitting of the data and allows the determination of the individual emission decays and energy gap between the singlet and triplet states. Corresponding fitting parameters are listed in Table 1. The obtained ΔE values for 1-3 are roughly consistent with the spectral shifts of 700-1600 cm^{-1} between 298 and 77 K, indicating that the two-state model is reasonable for this temperature range. This distinct ΔE value can be explained by the spatial separation between HOMO and LUMO, as discussed below. An analysis of obtained data allows us to come to a better understanding of the emission process. All complexes exhibit small values for the singlet–triplet splitting and therefore show pronounced TADF at ambient temperature. At room temperature, the emissions of complexes 1-3 occur mainly from the singlet state by efficient up-conversion, at 77 K emission occurs from the triplet state. Kinetically, the TADF/phosphorescence proportions at 300K have been assessed using following expression (2):[48]

$$\frac{I(T_1)}{I_{tot}} = \left(1 + \frac{QY(S_1)\tau(T_1)}{3QY(T_1)\tau(S_1)}\exp\left(-\frac{\Delta E}{k_B T}\right)\right)^{-1} \quad (2)$$

The percentage of phosphorescence to the whole emission of 2 and 3 at 300 K is practically negligible while in the case of 1 at room temperature, the ratio of TADF to the phosphorescent emission pathways is comparable. This is probably related to the lowering of the emission quantum efficiency of complex 1 because a larger population in the triplet state with smaller radiative rate constant (i.e. longer lifetime) should be more affected by the nonradiative decay. Thus, chorine complex 1 with the largest ΔE has the lowest quantum efficiency among the three complexes. On the other hand, almost 100% quantum yield is achieved by not only chloride but bromide complex with the smaller ΔE, even though the value is not so small compared to those reported. This proves the superior properties of these simple mononuclear complexes.

In addition to the TADF luminescence title complexes also exhibit the mechanoluminescence property. Upon grinding the crystalline samples of 1-3 in agate mortar significant change in the color of the emission from green to orange emission was observed (Fig.5). The luminescence became less intense and wavelength maximum shifted bathochromically to 596 nm (QY = 0.07), 600 (QY = 0.34) and 605 nm (QY = 0.16) respectively (Fig.6 a). Further we found that ground orange emission converted back to the initial green emission by or slight heat or exposure to acetonitrile vapors (Fig.6 b)

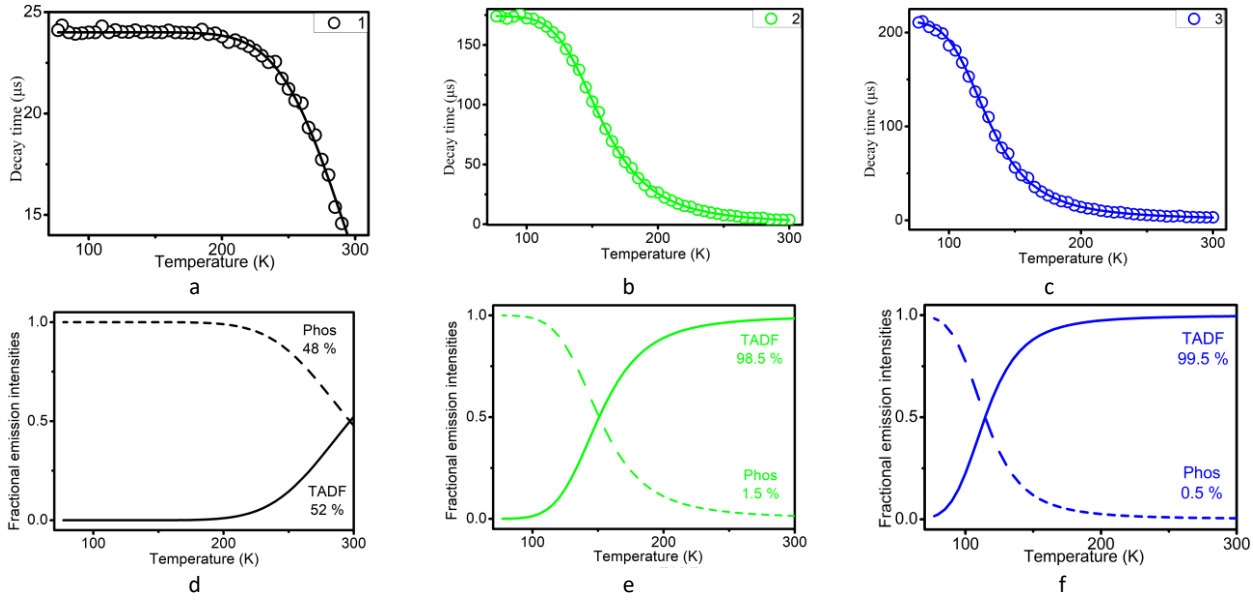

Figure 4. Temperature dependence of the emission decay time of complexes 1 (a), 2 (b) and 3 (c) and fit according to Eq. 2. Fractional emission intensities (simulation results) stemming from TADF and direct Phos. as a function of temperature for complexes 1 (d), 2 (e) and 3 (f), respectively, calculated according to Eq. 3. on the basis of the experimental data

This journal is © The Royal Society of Chemistry 20xx

Please do not adjust margins

Please do not adjust margins

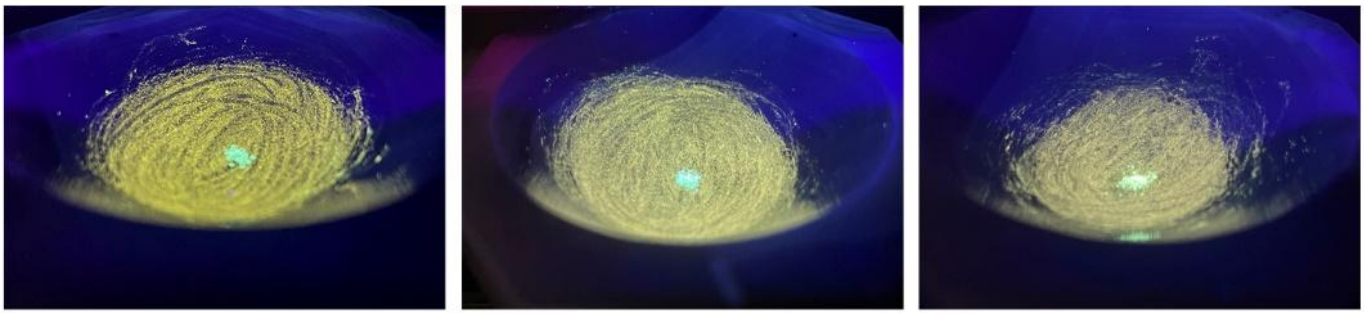

Figure 5. Photographs of single crystals and ground samples of 1-3 under UV light.

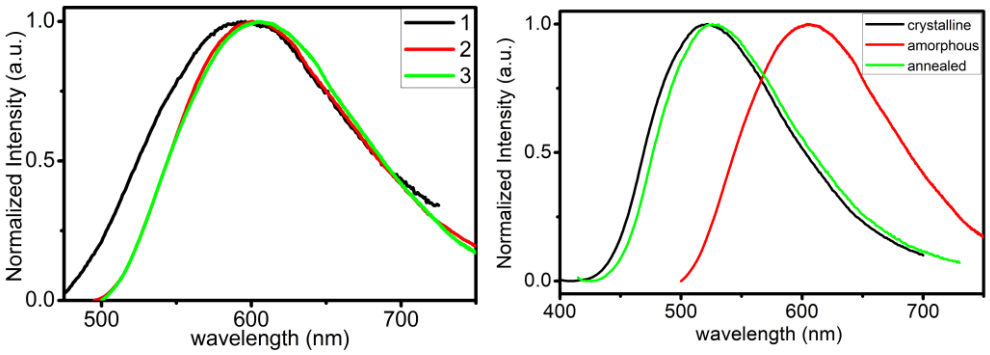

Figure 6. Emission spectra of amorphous samples 1-3 (a), Emission spectra of crystalline, amorphous, and annealed forms of 3.

Elemental analyses of 1-3 before and after grinding revealed the same chemical composition. Further IR spectra of pristine and ground samples were measured. The obtained data indicate that the spectral fingerprints in the remain unchanged, which also confirm the absence of molecular structural changes of complexes.

To gain an in-depth understanding of structure-property relationship of these mechanochromic complexes, the analysis of powder X-ray diffraction (PXRD) of the pristine, amorphous, and annealed samples 3 was conducted. As shown in Fig. 7, the pristine solids show sharp and intense reflections, indicative of the well-ordered microcrystalline structures. In contrast, the ground solids display broad and weak peaks, indicating that mechanical grinding destroy original crystalline structures of the complex into amorphous phase. After short annealing, sharp diffraction peaks similar to those of the pristine solids appeared again, suggesting the regeneration of the microcrystalline structures.

Totally amorphous phases of 1-3, were obtained by melting and fast cooling the crystalline phase. Amorphous glasses demonstrate luminescence spectra completely coincides with the spectra of ground complexes. Differential scanning calorimetry (DSC) analyses for the amorphous and crystalline states of 1, 2 and 3 show that the ground samples present an obvious exothermal peak at approximately 115 for 1, 103 for 2 and at 101 and 112 °C for 3, respectively, indicating a cold crystallization of the metastable amorphous state to more stable crystalline state or annealing state. Thus, the reversibility of luminescence in crystal-glass equilibrium is determined by the reversibility of the transition of states to each other. We consider that reversible changes in the properties of complexes during the transition from crystalline to amorphous states can be related to the destruction of specific intermolecular interactions, primarily hydrogen bonds.

Generaly by comparing the photophysical properties of 1-3 in various temperatures and forms, several information or expectations may be obtained. Firstly, the photophysical properties, including maximum emission wavelength, PLQY and decay lifetimes, are very sensitive to halide anion coordinated to copper cation. It is correlated with the sequence of increasing of π-accepting properties of halide ions (Cl^- < Br^- < I^-) leading to the increase in the energy gap between the excited and ground states and as results shifting of emission maxima. Moreover, in the Cl-Br-I series there is a tendency to decrease the energy gap between the singlet and triplet excited states of the corresponding complexes, which contributes to the realization of the TADF emission mechanism. Moreover, the realization of specific hydrogen bonds with the participation of halogens in crystals and its destruction during amorphization of complexes 1-3 is an effective way to tune their photophysical properties. This factor can be used for the purposeful search of new ways to control the emission properties of copper complexes.

This journal is © The Royal Society of Chemistry 20xx

Please do not adjust margins

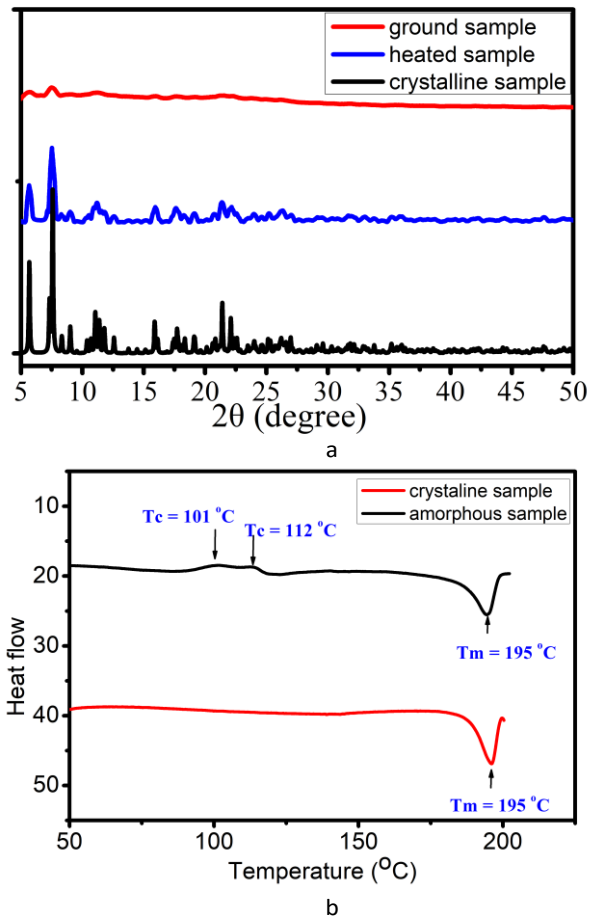

Figure 7. (a) Powder X-ray diffraction patterns of pristine, amorphous and annealed samples 3. (b) DSC curves of 3 in crystalline and amorphous states.

Theoretical Calculations

In accordance with the X-ray structural data, ground state optimization of all complexes confirm tetragonal coordination geometry for central Cu atom (Table 2 and Fig. 8). Optimized S_1 and T_1 states possess similar to ground singlet state geometries. However, for complex 1, the deviations in the N1-Cu1-P2 and P1-Cu1-P2 angles between the S_0 and S_1 optimized geometries are considerable and equal to 27° and 18° (Table 2), respectively. The corresponding deviations for the remaining two complexes vary in smaller region 4-11° which reveals that the structural transformations are not identical for the three complexes. However, these structural differences have a profound effect on the predicted energetic characteristics like ΔE_{ST} and reorganization energies for complex 1 that are predicted to be highest among the three complexes. This results in less probability of reverse intersystem crossing (RISC) and thus in less efficient TADF in line with experimental observations. The oscillator strengths (f) of the $S_0 \leftarrow S_1$ transition are almost identical for 2 and 3 complexes at the S_1 optimized geometry and significantly increased for 1 resulting in a substantial increase in the predicted fluorescence rate (k_f) (Table 3).

For a better understanding of the luminescence of the complexes 1-3, density functional theory (DFT) and Tamm-Dancoff approximation to time-dependent DFT (TDA-TDDFT) calculations were performed. Table 3 combines the computed fluorescence, phosphorescence wavelengths and triplet-singlet energy difference (eV) (for both restricted ΔE_{ST} and unrestricted ΔES_{UT} triplet state calculations).

The orbital nature of S_1 and T_1 states for all three complexes are very similar and do not actually changed upon geometry relaxation in S_1 or T_1 state. HOMO is mainly localized on the halogen atoms and Cu central atom with some small contribution on triphenylphosphane fragment, while the LUMO is located on the 3-phenyl-5-(pyridin-4-yl)-1,2,4-triazole ligand. Thus, we assign the S_1 and T_1 states of all complexes to the ligand-to-ligand charge-transfer (LLCT) with some contribution of metal-to-ligand charge transfer (MLCT). The adiabatic energy gaps calculated by two different approaches for T_1 state energy (ΔE_{ST} and ΔE_{SUT}, more details in SI) were found to be similar meaning applicability of both spin-restricted TDA-TDDFT/PBE0 and spin-unrestricted UPBE0 approaches for ΔE_{ST} estimations. Our simulations also reproduce well the fluorescence maxima observed in experimental measurements.

Combining the calculated values of adiabatic singlet-triplet energy differences, reorganization energies, and computed spin-orbit coupling matrix elements (SOCMEs) within the semiclassical Marcus theory expression,[49] we have predicted the rates of ISC (k_{ISC}) to be at the levels of 6.39×10^{10}, 5.69×10^{9}, and 8.88×10^{9} S^{-1} for complexes 1, 2 and 3, respectively (Table 3). While, for the reverse ISC process, we estimated k_{RISC} values to be equal to 2.82×10^{7}, 8.04×10^{8}, and 1.14×10^{9} S^{-1}, respectively (Table 3). The photophysical pattern of the delayed fluorescence phenomenon in the complexes can be characterized accordingly: the rate of ISC is much faster than the rate of fluorescence k_f, and thus prompt fluorescence is suppressed by the ISC. Consequently, the rate-determining step of the emissive TADF relaxation pathway is the reverse intersystem crossing rate which was found to be slowest for complex 1. The ratio between k_{ISC} and k_{RISC} actually defines the efficiency of TADF and in agreement with experimental measurements: 1 demonstrate weakest TADF comparing to the 2 and 3 complexes. The phosphorescence of the complexes is predicted to be a process that is too slow to compete with the fluorescence channel under room-temperature conditions.

Table 2. Selected geometric parameters of 1, 2, and 3 complexes optimized in acetonitrile solvent (CH_3CN) using DFT/PBE0 for ground and TDA-TDDFT for excited state with 6-311G(d,p) basis set and LanL2DZ ECP for Cu and halogens (X).

Complex	Bonds (Å)				Angles (˚)		
	Optimized Ground State (S_0)						
	Cu1-X	Cu1-P1	Cu1-P2	Cu1-N1	N1-Cu1-P2	N1-Cu1-P1	P1-Cu1-P2
1	2.43	2.31	2.33	2.15	99	108	123
2	2.65	2.40	2.41	2.18	106	109	125
3	2.73	2.32	2.33	2.14	100	109	122
Excited State (S_1)							

This journal is © The Royal Society of Chemistry 20xx

1	2.38	2.35	2.37	2	126	101	105
2	2.47	2.39	2.39	1.98	95	105	131
3	2.64	2.38	2.39	1.99	96	105	132

Table 3. Computed fluorescence (λ_{fl} nm), phosphorescence (λ_{phos}, nm), singlet-triplet energy difference (ΔE_{ST} and ΔE_{SUT} eV), reorganization energies (λ_S and λ_T, eV), and constants of 1-3 in acetonitrile solvent (CH_3CN) using TDA-TDDFT/PBE0 method and combined basis set: 6-311G(d,p) for light atoms and Lanl2DZ for Cu, Cl, Br and I.

Complex	λ_{fl}, nm (*f*)	λ_{phos}, nm	E_{ST}, eV	ΔE_{SUT}, eV	λ_S, eV	λ_T, eV	k_f, s^{-1}	k_p, s^{-1}	k_{ISC}, s^{-1}	k_{RISC}, s^{-1}
1	553 (0.03)	635	0.252	0.314	0.195	0.138	6.22×10^{6}	4.23×10^{2}	6.39×10^{10}	2.82×10^{7}
2	589 (0.014)	611	0.157	0.216	0.082	0.033	2.19×10^{6}	2.94×10^{2}	5.69×10^{9}	8.04×10^{8}
3	572 (0.02)	586	0.146	0.205	0.087	0.032	2.86×10^{6}	4.4×10^{3}	8.88×10^{9}	1.14×10^{9}

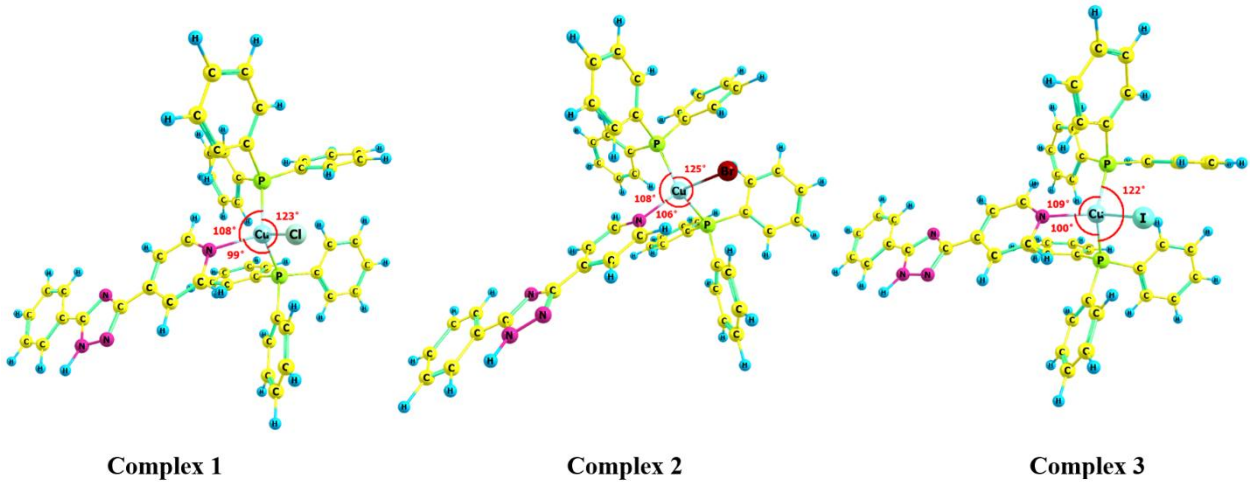

Figure. 8. Ground state molecular structures of 1-3 optimized with DFT-B3LYP level of theory and 6-311G(d, p) basis set for C, P, O, N, and H, and LANL2DZ for Cu and halogen atoms.

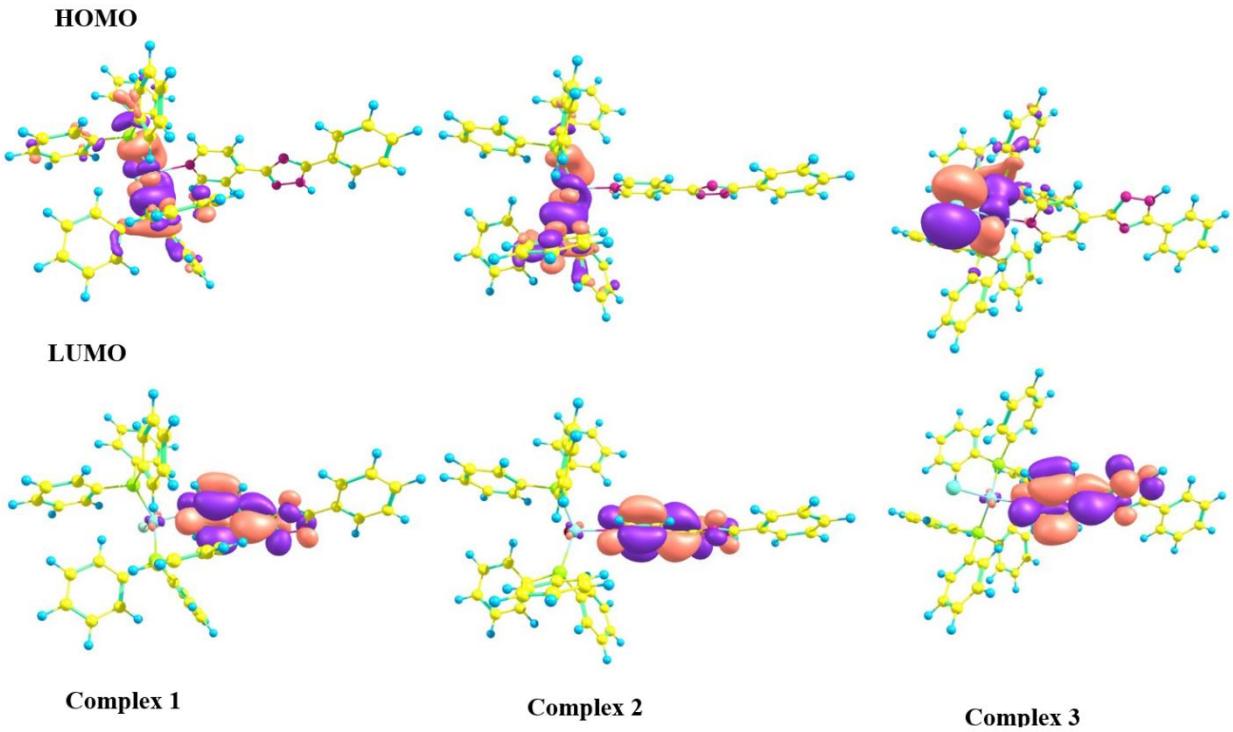

Figure 9. The ground-state frontier molecular orbitals of 1-3 computed with DFT-B3LYP level of theory and 6-311G(d, p) basis set for C, P, O, N, and H, and LANL2DZ for Cu and halogen atoms.

ARTICLE

OLED performance

The high intensity and efficiency of photoluminescence as well as quite pure green emission of complexes 1-3 motivated us to use them as emitters in OLED cells as more accessible analogs of famous green emissive Ir(III) complexes.[50] In order to select materials for additional layers of OLED cells in the first step, the energy values of frontier orbitals were evaluated from electrochemical data and UV-vis data of 1-3 (Table S5). Using the obtained data and taking into account OLED structures previously used to realize the electroluminescence of similar copper complexes [51-54], we proposed the following architecture: ITO (100 nm)/PEDOT:PSS(40nm)/PYD-2Cz/1, 2 or 3(10wt%)(30 nm)/TPBi (60 nm)/LiF(1nm)/Al(80nm). Herein, PEDOT:PSS (poly(3,4-ethylenedioxythiophene) polystyrene sulfonate) and TPBi (1,3,5-Tris(1-phenyl-1Hbenzimidazol-2-yl)benzene) were utilized as a hole-transport layer and an electron-transport layer, respectively. The host material PYD-2Cz (2,6-Di(9H-carbazol-9-yl)pyridine) were utilized to balance the charge carrier transport and to expand the exciton recombination region. Since the studied Cu(I) complexes are not stable enough for vacuum deposition technique of device fabrication, we used these complexes as emitting dopants to fabricate OLEDs through the solution process. The hole-injection and emitting layers were prepared by spin coating procedure also. The remaining layers were deposited by vacuum thermal evaporation (see detail in ESI). Fig. 10 shows the schematic energy-level diagram and structure configurations of the organic materials.

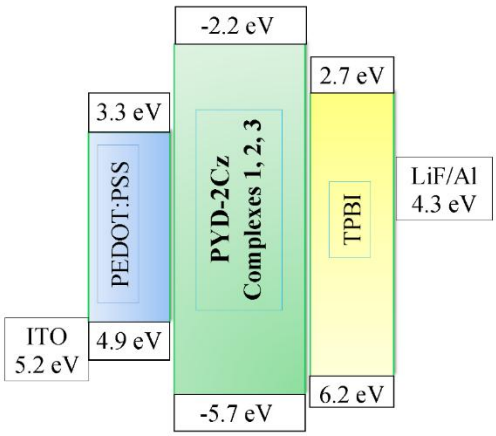

Figure.10. The energy diagram of devices 1, 2 and 3

The choice of organic layers was made taking into account the close values of the boundary orbital energies, providing balanced charge recombination with the advantage in suppressing energy losses during the host-dopant energy transfer. The bright green light emit from the devices with emission peaks centered at 545 nm for 1, 530 nm for 2 and 524 nm for 3 (Fig 11. a). No emissions from the host or other layers were observed confirming that charge carrier recombination is completely confined to the emissive layer. The luminescence intensity increased with an increase in the injection current as well as bias voltage. It is noteworthy that the electroluminescence spectra are slightly narrowed in comparison with photoluminescent ones, which may be due to the leveling of the intermolecular interaction in the thin films. Commission Internationale de L'Eclairage (CIE) coordinates (Table 4) correspond to almost pure green, which allows us to recommend complexes 1-3 as an alternative to the traditional iridium complexes.[50]

The EL performance parameters of devices 1, 2 and 3 are depicted in Fig. 11 b-d and collected in Table 4. By comparing the three OLEDs, it is found that the device 2 demonstrates the best performance, with EQE reaching 13.5% (31.9 cd/A) at 200 cd/m^2 and 8.7% (19.3 cd/A) at 2000 cd/m^2. The power efficiency reaches 25.7 lm/W at 200 cd/m^2 and 18.8 lm/W at 2000 cd/m^2, which is comparable to OLEDs with iridium based phosphors. The maximum brightness of electroluminescence reaches 3260, 4610, and 3220 Cd m^{-2} for devices 1, 2 and 3, respectively. Although these values are not record-breaking for copper complexes [29], nevertheless, taking into account the high emission efficiency, they allow us to recommend the synthesized compounds for commercial use. It is likely that the brightness and efficiency of these devices can be further optimized.

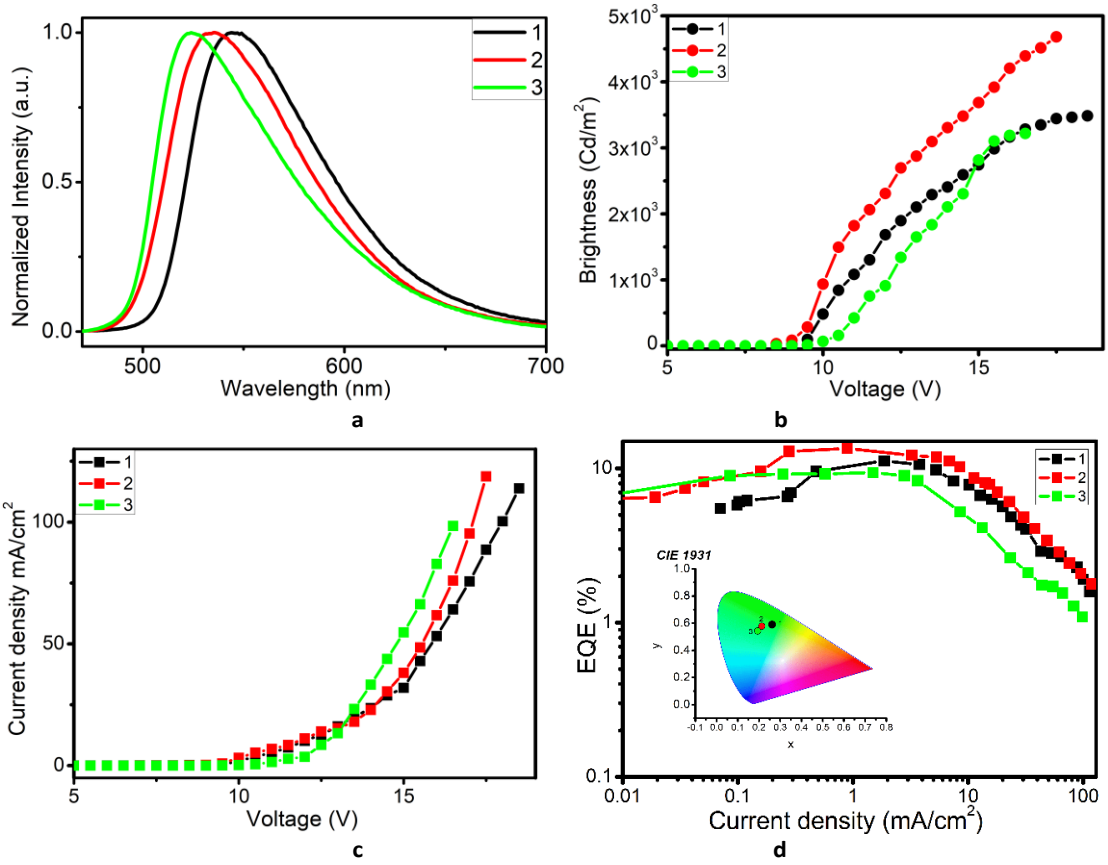

Figure.11. a) Electroluminescence spectra of devices 1-3; b) brightness as a function of applied voltage of devices 1-3; c) current density as a function of applied voltage of devices 1-3; d) External quantum efficiency (EQE) as a function of current density (Inset: CIE coordinates of devices 1-3).

Table 4. Performance of OLED devices 1-3 based on complexes 1, 2, 3, respectively.

Device	Turn on voltage, V	Max. rightness, cd/m^2	Max. current efficiency, cd/A	External quantum efficiency, %	CIE coordinates (X, Y)
Device 1	9.0	3480	25.8	11.2	0.29; 0.60
Device 2	8.5	4680	31.9	13.5	0.25; 0.59
Device 3	10.0	3220	27.7	9.4	0.21; 0.51

Conclusions

Mononuclear CuX (X = Cl, Br, I) complexes of PPh_3 with 3-phenyl-5-(pyridin-4-yl)-1,2,4-triazole were synthesized. Synthesized complexes demonstrate green emitting in crystalline at room temperature, for which their crystal structures and emission nature have been identified by X-ray diffraction structure analysis, photophysical studies and theoretical calculations. The emission studies and TD-DFT calculations reveal that complexes 1-3 emit TADF from the ^{1}(M+L)LCT state at room temperature because of small singlet–triplet energy gaps and considerable spin-orbit coupling effects. Complexes demonstrate very high quantum yield of emission both at 77 and 298 K. Besides this, luminescence mechanochromism, corresponding to crystalline-to-amorphous transition, was also found for this series of complexes. By using the studied complexes as emissive components a series of doped highly efficient green-emitting OLEDs was fabricated. Resulting performance of designed OLEDs reveals complexes 1-3 as promising emitting components of organic lighting systems.

Acknowledgment

Conflicts of interest

There are no conflicts to declare.

Acknowledgements

The authors (A.G., E.B., E.Z.) would like to acknowledge the financial support from Russian Science Foundation grant (project no. 22-73-00043). A.A. and G.B. thank for support from Carl Tryggers Stiftelse (Sweden), project number CTS 21:1430. G.B. thanks the support by the Swedish Research Council through starting grant No. 2020-04600. The quantum-chemical calculations were performed with computational resources

Please do not adjust margins

provided by National Academic Infrastructure for Supercomputing in Sweden (NAISS 2023/5-77) at the National Supercomputer Centre (NSC) at Linköping University partially funded by the Swedish Research Council through grant agreement no. 2022-06725. Single crystal X-ray diffraction analysis was performed using the equipment at the Center for Collective Use of the Kurnakov Institute RAS, which operate with the support of the state assignment of the IGIC RAS.

References

1 N. Mirzadeh, S. H. Priver, A. J.Blake, H. Schmidbaur, S. K. Bhargava, Innovative molecular design strategies in materials science following the aurophilicity concept. *Chemical reviews* 2020**, 120** (15), 7551.

2 Z. Yang, Z. Mao, Z. Xie, Y. Zhang, S. Liu, J. Zhao, J. Xu, Z. Chi, M. P. Aldred, Recent advances in organic thermally activated delayed fluorescence materials. *Chem. Soc. Rev.* 2017**, 46 (3**), 915.

3 W. Wang, Y. Zhang, W. J. Jin, Halogen bonding in room-temperature phosphorescent materials. *Coord. Chem. Rev.* 2020**, 404**, 213107.

4 V.-N. Nguyen, A.Kumar, M. H. Lee, J. Yoon Recent advances in biomedical applications of organic fluorescence materials with reduced singlet–triplet energy gaps. *Coord. Chem. Rev.* 2020**, 425**, 213545.

5 H.-Y. Li, S.-N. Zhao, S.-Q. Zang, J. Li, Functional metal–organic frameworks as effective sensors of gases and volatile compounds. *Chem.Soc. Rev.* 2020**, 49** (17), 6364.

6 M. D. Smith, B. A. Connor, H. I. Karunadasa, Tuning the luminescence of layered halide perovskites. *Chemical Reviews* 2019**, 119** (5), 3104.

7 J. M. Ha, S. H. Hur, A. Pathak, J.-E. Jeong, H. Y. Woo, Recent advances in organic luminescent materials with narrowband emission. *NPG Asia Materials* 2021**, 13** (1), 53.

8 S. Lee, W.-S. Han, Cyclometalated Ir (III) complexes towards blue-emissive dopant for organic light-emitting diodes: fundamentals of photophysics and designing strategies. *Inorganic Chemistry Frontiers* 2020**, 7** (12), 2396-2422.

9 H. Amouri, Luminescent Complexes of Platinum, Iridium, and Coinage Metals Containing N-Heterocyclic Carbene Ligands: Design, Structural Diversity, and Photophysical Properties. *Chem. Rev.* 2023, **123**, 230

10 M. S. Alsaeedi, Insight into luminescent iridium complexes: Their potential in light-emitting electrochemical cells. *J. of Saudi Chem. Soc.* 2022, 101442.

11 Z. Liu, Z. Bian, C. Huang, Luminescent iridium complexes and their applications. *Molecular organometallic materials for optics* 2010, 113.

12 M. Kinzhalov, K. Luzyanin, Synthesis and Contemporary Applications of Platinum Group Metals Complexes with Acyclic Diaminocarbene Ligands. *Russ. J. of Inorg. Chem.* 2022**, 67** (1), 48.

13 J. G. Williams, S. Develay, D. L. Rochester, L. Murphy, Optimising the luminescence of platinum (II) complexes and their application in organic light emitting devices (OLEDs). *Coord. Chem.Rev.* 2008**, 252** (23-24), 2596.

14 Y. Chi, P.-T. Chou, Transition-metal phosphors with cyclometalating ligands: fundamentals and applications. *ChemSocRev* 2010**, 39** (2), 638.

15 A. N. Gusev, M. A. Kiskin, E. V. Braga, M. A. Kryukova, G. V. Baryshnikov, N. N. Karaush-Karmazin, V. A. Minaeva, B. F. Minaev, K. Ivaniuk, P. Stakhira, Schiff base zinc (II) complexes as promising emitters for blue organic light-emitting diodes. *ACS Applied Electronic Materials* 2021**, 3** (8), 3436.

16 A. S. Burlov, V. G. Vlasenko, M. S. Milutka, Y. V. Koshchienko, N. I. Makarova, V. A. Lazarenko, A. L. Trigub, A. A. Kolodina, A. A. Zubenko, A. V. Metelitsa, D. A. Garnovskii, A. N. Gusev, W. Linert, Synthesis, Structure, Spectral-Luminescent Properties, and Biological Activity of Chlorine-Substituted N-[2-(Phenyliminomethyl) phenyl]-4-methylbenzenesulfamide and Their Zinc (II) Complexes. *Inter. J. of Mol. Sciences* 2022**, 23**, 15259.

17 F. Dumur, E.Contal, G. Wantz, D. Gigmes, Photoluminescence of zinc complexes: Easily tunable optical properties by variation of the bridge between the imido groups of Schiff base ligands. *Eur. J. of Inorg. Chem.* 2014**, 2014** (25), 4186.

18 X. Yan, X. Song, X. Mu, Y. Wang Mechanochromic luminescence based on a phthalonitrile-bridging salophen zinc (II) complex. *NJC,* 2019**, 43** (40), 15886.

19 C.-H. Huang, M. Wen, C.-Y. Wang, Y.-F. Lu, X.-H. Huang, H.-H. Li, S.-T. Wu, N.-F. Zhuang, X.-L. Hu, A series of pure-blue-light emitting Cu (i) complexes with thermally activated delayed fluorescence: structural, photophysical, and computational studies. *Dalton Trans.,* **2017, 46** (5), 1413.

20 B. A. Babgi,, Synthetic protocols and applications of copper (I) phosphine and copper (I) phosphine/diimine complexes. *J. of Organometallic Chemistry,* 2021**, 956**, 122124.

21 L.-T. Wang, Z.-Z. Ma, F. Zhang, M. Wang, X. Chen, D. Wu, Y.-T. Tian, X.-J. Li, Z.-F. Shi, Stable down-conversion white light-emitting devices based on highly luminescent copper halides synthesized at room temperature. *J. of Materials Chemistry C* 2021**, 9** (19), 6151.

22 V. K.-M. Au, Organic light-emitting diodes based on luminescent self-assembled materials of copper (I). *Energy & Fuels* 2021**, 35** (23), 18982.

23 J. Troyano, F. Zamora, S. Delgado, Copper (I)–iodide cluster structures as functional and processable platform materials. *ChemSocRev*. 2021**, 50** (7), 4606.

24 A. Kobayashi, M. Kato, Stimuli-responsive luminescent copper (I) complexes for intelligent emissive devices. *Chem. Lett.* 2017**, 46** (2), 154.

25 E. Cariati, E. Lucenti, C. Botta, U. Giovanella, D. Marinotto, S. Righetto, Cu(I) hybrid inorganic–organic materials with intriguing stimuli responsive and optoelectronic properties. *Coord. Chem.Rev.* 2016**, 306**, 566.

26 P. C. Ford, E. Cariati, J. Bourassa, Photoluminescence properties of multinuclear copper (I) compounds. *Chem.rev.* 1999**, 99** (12), 3625.

27 K. Tsuge, Y. Chishina, H. Hashiguchi, Y. Sasaki, M. Kato, S. Ishizaka, N. Kitamura, Luminescent copper (I) complexes with halogenido-bridged dimeric core. *Coord. Chem. Rev.* 2016**, 306**, 636-651.

28 A. Tsuboyama, K. Kuge, M. Furugori, S. Okada, M. Hoshino, K. Ueno, Photophysical properties of highly luminescent copper (I) halide complexes chelated with 1, 2-bis (diphenylphosphino) benzene. *Inorg. chem.* 2007, ***46*** (6), 1992.

29 C. E. Housecroft, E. C. Constable TADF: Enabling luminescent copper(I) coordination compounds for light-emitting electrochemical cells. *J. of Materials Chemistry C* 2022**, 10** (12), 4456.

30 N. Armaroli, Photoactive mono-and polynuclear Cu (I)–phenanthrolines. A viable alternative to Ru (II)–polypyridines? *Chem. Soc. Rev.* 2001**, 30** (2), 113.

31 M. Ruthkosky, C. A. Kelly, F. N. Castellano, G. J.nMeyer, Electron and energy transfer from CuI MLCT excited states. *Coord. chem. rev.* 1998**, 171,** 309.

32 C. Sandoval-Pauker, M.nSantander-Nelli, P. Dreyse, Thermally activated delayed fluorescence in luminescent cationic copper (I) complexes. *RSC adv,* 2022**, *12*** (17), 10653.

33 H. Xu, T. Yang, F. Wang, J. Zhang, X. Zhang, H. Wang, B.Xu, Thermally activated delayed fluorescence of copper (I)

 This journal is © The Royal Society of Chemistry 20xx

Please do not adjust margins

Please do not adjust margins

complexes using N, N'-heteroaromatic of 2-(5-phenyl-1,2,3-triazole) pyridine as ligand. *J. of Luminescence* 2019**, 205**, 82.

34 a) A. Gusev, E. Braga, E. Zamnius, M. Kiskin, M. Kryukova, A. Baryshnikova, B. Minaev, G. Baryshnikov, H. Ågren, W.Linert, Structure and excitation-dependent emission of novel zinc complexes with pyridyltriazoles. *RSC adv* 2019**, 9** (38), 22143; b) A. Gusev, E. Braga, Y. Baluda, M. Kiskin, M. Kryukova, N. Karaush-Karmazin, G. Baryshnikov, A. Kuklin, B. Minaev, H. Ågren, Structure and tuneable luminescence in polymeric zinc compounds based on 3-(3-pyridyl)-5-(4-pyridyl)-1, 2, 4-triazole. *Polyhedron* 2020**, 191**, 114768.

35 A. Gusev, V. Shul'gin, E. Braga, E. Zamnius, M. Kryukova, W. Linert, Luminescent properties of Zn complexes based on tetradentate N2O2-donor pyrazolone schiff bases, *Dyes & Pigm*. 2020, **183**, 108626.

36 L. Krause, R. Herbst-Irmer, G.M. Sheldrick, D. Stalke, Comparison of silver and molybdenum microfocus X-ray sources for single-crystal structure determination. *J. Appl. Cryst.* 2015, **48**, 3.

37 a) G. M. Sheldrick, Crystal structure refinement with SHELXL. *Acta Crystallographica Section C: Structural Chemistry* 2015**, 71** (1), 3 b) A. L. Spek, PLATON SQUEEZE: a tool for the calculation of the disordered solvent contribution to the calculated structure factors. *Acta Cryst. Sect. C: Structural Chemistry* 2015**, 71** (1), 9.

38 G. A.Bowmaker, P. C. Healy, J. D. Kildea, A. H. Whites Far infrared spectroscopy of complexes of copper(I) halides with phosphine and amine ligands. *Spectrochimica Acta Part A: Molecular Spectroscopy,* 1988, **44**, 1219.

39 A. Gusev, M. Kiskin, E. Braga, E. Zamnius, M. Kryukova, N. Karaush-Karmazin, G. Baryshnikov, B. Minaev, W.Linert, Structure and emission properties of dinuclear copper(I) complexes with pyridyltriazole. *RSC Adv*., 2023, **13**, 3899

40 L. Yang, D.R. Powell, R.P. Houser Structural variation in copper(I) complexes with pyridylmethylamide ligands: structural analysis with a new four-coordinate geometry index, τ4, *Dalton Trans*., 2007, 955.

41 L. Wang, Y. Guo, B. Yu, W. Zhang, T. Li, J. Qu Simple cuprous iodide complex-based crystals with deep blue emission and high photoluminescence quantum yield up to 100%, *Appl Organometal Chem*. 2019**,** e4731.

42 H. Ohara, A. Kobayashi, M. Kato, Simple and Extremely Efficient Blue Emitters Based on Mononuclear Cu(I)-Halide Complexes with Delayed Fluorescence, *Dalton Trans.,* 2014, **43**, 17317.

43 S. Shi, M.C. Jung, C. Coburn, A. Tadle, M.R.D., Sylvinson, P.I. Djurovich. S. R. Forrest, M. E. Thompson. Highly efficient photo- and electroluminescence from two-coordinate Cu(I) complexes featuring nonconventional N-heterocyclic carbenes. *J Am Chem Soc*. 2019, **141**(8), 3576.

44 L. Lin, D-H. Chen, R. Yu, X-L Chen, W-J. Zhu, D. Liang. J.-F.Chang, Q. Zhang, C.-Z. Lu. Photo- and electroluminescence of three TADF binuclear Cu(i) complexes with functional tetraimine ligands. *J Mater Chem C.* 2017, ***5***(18), 4495

45 A. Kobayashi, Y. Yoshida, M. Yoshida, M. Kato. Mechanochromic switching between delayed fluorescence and phosphorescence of luminescent coordination polymers composed of dinuclear copper(I) iodide rhombic cores. *Chem Eur J,* 2018, **24**(55), 14750.

46 J.R. Lakowicz, Principles of fluorescence spectroscopy, 3rd ed., Springer, New York, 2006, 141-143.

47 T. Hofbeck, H. Yersin, The Triplet State of fac-Ir(ppy)3. *Inorg. Chem*. 2010, **49**, 9290

48 M. J. Leitl, F.-R. Küchle, H. A. Mayer, L. Wesemann, H. Yersin, Brightly Blue and Green Emitting Cu(I) Dimers for Singlet Harvesting in OLEDs, *J. Phys. Chem. A* 2013, **117**(46) 11823

49 Marcus, R. A., Electron transfer reactions in chemistry: theory and experiment (Nobel lecture). *Angew. Chem. Inter. Ed.* 1993**, 32**(8), 1111.

50 C. E. Housecroft, E. C. Constable Over the LEC rainbow: Colour and stability tuning of cyclometallated iridium(III) complexes in light-emitting electrochemical cells. *Coord. Chem. Rev*., 2017, **350**, 155.

51 F. Dumur, Recent advances in organic light-emitting devices comprising copper complexes: A realistic approach for low-cost and highly emissive devices?. *Organic Electronics*, 2015, **21**, 27.

52 Z. Liu, J. Qiu, F. Wei, J. Wang, X. Liu, M. G. Helander, S. Rodney, Z. Wang, Z. Bian, Z.Lu, M. E. Thompson, C. Huang, Simple and High Efficiency Phosphorescence Organic Light-Emitting Diodes with Codeposited Copper(I) Emitter. *Chem. Mater*. 2014, **26***,* 2368.

53 Z. Liu, M. F. Qayyum, C. Wu, M. T. Whited, P. I. Djurovich, K. O. Hodgson, B. Hedman, E. I. Solomon, M. E. Thompson, A codeposition route to CuI−pyridine coordination complexes for organic light-emitting diodes. *J. Am. Chem. Soc.* 2011, **133***,* 3700

54 V.K.-M. Au, Organic Light-Emitting Diodes Based on Luminescent Self-Assembled Materials of Copper(I). *Energy Fuels* 2021, **35**, 18982.

Please do not adjust margins